SCIENTIFIC REPORTS

OPEN

SUBJECT AREAS:
ENERGY
CHEMICAL ENGINEERING
OPTICAL METROLOGY
KINETICS AND DYNAMICS

Received
3 July 2013

Accepted
4 February 2014

Published
19 February 2014

Correspondence and requests for materials should be addressed to C.-Y.S. (cysun@cup.edu.cn); G.-J.C. (gjchen@cup.edu.cn) or A.K.S. (asum@mines.edu)

New Observations and Insights into the Morphology and Growth Kinetics of Hydrate Films

Sheng-Li Li[1], Chang-Yu Sun[1], Bei Liu[1], Zhi-Yun Li[1], Guang-Jin Chen[1] & Amadeu K. Sum[2]

[1]State Key Laboratory of Heavy Oil Processing, China University of Petroleum, Beijing, 102249, China, [2]Center for Hydrate Research, Chemical & Biological Engineering Dept., Colorado School of Mines, Golden, CO 80401, USA.

The kinetics of film growth of hydrates of methane, ethane, and methane-ethane mixtures were studied by exposing a single gas bubble to water. The morphologies, lateral growth rates, and thicknesses of the hydrate films were measured for various gas compositions and degrees of subcooling. A variety of hydrate film textures was revealed. The kinetics of two-dimensional film growth was inferred from the lateral growth rate and initial thickness of the hydrate film. A clear relationship between the morphology and film growth kinetics was observed. The shape of the hydrate crystals was found to favour heat or mass transfer and favour further growth of the hydrate film. The quantitative results on the kinetics of film growth showed that for a given degree of subcooling, the initial film thicknesses of the double hydrates were larger than that of pure methane or ethane hydrate, whereas the thickest hydrate film and the lowest lateral growth rate occurred when the methane mole fraction was approximately 0.6.

Natural gas hydrates are a potential energy resource with huge reserves[1]. Gas hydrates can also find use in gas storage[2–4], transportation[5–7], and gas mixture separation[8]. However, gas hydrates may pose a plugging hazard during the production and transportation of crude oil and natural gas. Understanding the kinetic rate of gas hydrate formation is fundamental to both the utilisation of gas hydrates and the prevention of gas hydrate formation. In general, gas hydrate formation initiates at the water/guest-fluid interface. Once a hydrate crystal forms at the interface, it can grow along the lateral and normal directions to the interface, thereby forming a hydrate film with a certain thickness between the water and guest fluid[9,10].

The morphology and growth rate of the hydrate film at the water/guest-fluid interface are significant to the overall study of hydrate formation kinetics. The morphologies of hydrates formed with a methane/ethane/propane gas mixture in bulk liquid water[11] and on the surface of a water droplet[12] were previously studied. In the study on hydrate crystal growth in bulk liquid water, it was found that the morphology of the hydrate crystals changed with the degree of subcooling and the methane mole fraction in the gas mixture[11]. In the study on hydrate crystal growth on the surface of a water droplet, it was found that the crystal size decreased with increasing methane concentration in the gas mixtures. In addition, the crystal size was smaller than that of simple methane hydrates[12]. The macroscopic crystal growth morphology for hydrates formed from a 89.4% methane/10.6% ethane mixture was also studied with an emphasis on the investigation of induction time for hydrate formation on water droplets[13]. It was observed that as the methane mole fraction changed by no more than 10%, the influence of gas composition on the hydrate morphology could not be clearly distinguished. More importantly, these studies focused on the morphology of hydrate crystals, while the relationship between morphology and film growth kinetics was not addressed.

The lateral growth of hydrate films at the gas/liquid or gas/solid interface has been studied experimentally and/or theoretically by several groups[9,14–19]. However, most reported studies are for simple hydrates formed from a single guest. The initial thickness and lateral growth rate of the hydrate film are the key quantities to be measured to obtain the volumetric hydrate growth rate, which is often very difficult to measure. Selected measurements for the thickening rate of hydrate films in the normal direction to the interface after initial lateral growth exist[20–23]. The reported techniques for measuring film thickening rate include micrometry, microscopy[20–23], laser interferometry[24], and the magnetic resonance imaging (MRI)[25]. Neither the laser interferometry nor MRI can determine the absolute initial thickness of the hydrate film, although they can determine the thickening rate to some extent. In our previous work[26], we developed a method to measure the initial thickness of a hydrate film formed on the surface of a gas bubble exposed in water using a microscopic camera. A series of initial thickness data for

methane hydrate films were measured using this method[26], and it was shown that the initial thickness of the hydrate film was inversely proportional to the degree of subcooling[19]. This finding is critical for modelling the lateral growth rate of the hydrate film based on the heat transfer control model proposed by Mori[15].

In this study, the film growth kinetics of simple ethane hydrates and methane-ethane double hydrates were visually studied, including the dependence of the morphology, lateral growth rate, and thickness of the hydrate film on the gas composition and degree of subcooling. This study aims to establish a relationship between hydrate morphology and film growth kinetics.

Results

The reported results are based on changes in the gas composition and degree of subcooling (ΔT_{sub}). The degree of subcooling is defined as $\Delta T_{sub} = T^{eq} - T^{exp}$, where T^{exp} is the experimental temperature and T^{eq} is the hydrate formation equilibrium temperature at the experimental pressure (calculated with the Chen-Guo hydrate model[27]). Generally, differences in the morphology of hydrate films formed by different gases are clear at lower degrees of subcooling but disappear at higher degrees of subcooling. Figure 1 and Figures S3 to S6 in the Supporting Material display diverse and texture-rich morphologies of hydrate films formed from eight groups of different gases at three different degrees of subcooling. The images shown in the figures are views of the hydrate films. All of the images were captured during lateral hydrate film growth or just after complete coverage of the gas bubble surface by the hydrate film.

According to Figure 1, it is very interesting that the morphologies of hydrate films formed by gas mixtures with methane mole fractions between 0.190 and 0.620 are similar to that of pure ethane hydrate films but are quite different from that of pure methane hydrate films. This observation suggests that for these systems, nucleation and growth of the hydrate crystal is dominated by ethane. The texture of hydrate films formed at lower degree of subcooling ($\Delta T_{sub} < 1$ K) is clear, with individual crystals commonly appearing as long and stratified features (for more details, see videos 1 to 3 in the Supporting Material). At higher degrees of subcooling ($2\ K < \Delta T_{sub} < 3$ K), the hydrate crystals are shorter and grain-like in shape (for more details, see videos 4 and 5 in the Supporting Material). As observed earlier, the size of the hydrate crystals decreases with increasing subcooling. This phenomenon is due to an increased rate of formation of new crystal seeds at higher degrees of subcooling. The emergence of new crystal seeds on the surface of a growing crystal hinders continued growth of a few large crystals at the expense of many small crystals[26]. Increasing the degree of subcooling therefore shortens the growth period of each crystal.

When the methane mole fraction of gas mixtures increases to 0.834 and even 0.923, the crystal morphology becomes leaf-like or dendritic (for more details, see videos 6 and 7 in the Supporting Material), which is significantly different from that of hydrate films formed from pure ethane, pure methane, and mixtures with the methane mole fraction ranging from 0.190 to 0.620. This difference may be attributed to the formation of structure II (sII) methane-ethane double hydrates[28–30]. The structural transition of methane-ethane double hydrates from structure I (sI) to sII has been demonstrated by Raman spectroscopy[31] and *in situ* neutron diffraction[28,32] for a methane composition range (y_{CH4}) of 0.72 to 0.75. Conversely, the transition from sII to sI occurs over a y_{CH4} range of 0.992 to 0.994[29,30,33]. The leaf-like morphology observed here is very similar to that of a sII hydrate film formed at a higher degree of subcooling ($\Delta T_{sub} \sim 3$ K) on the surface of the water droplet from a methane-ethane-propane (90 : 7 : 3 molar ratio) gas mixture[12]. The similarity of the results suggests that sII hydrates are being formed. Further determination of the structures of hydrate crystals would request Raman spectroscopy data in addition to the visual observations in this work.

It is very interesting to observe that the hydrate crystals formed at low degrees of subcooling ($\Delta T_{sub} < 1$ K) always tend towards shapes favorable for heat or mass transfer and further fast hydrate film growth. The formation of stratified crystals with peaks and valleys certainly increases the total interfacial area between the hydrate and water, and maximising heat transfer. The dendritic shape of the hydrate crystals facilitates both heat transfer and mass transfer. Mass transfer resistance may become a critical problem for gas mixtures with lower ethane concentrations. It has been shown that ethane can be easily removed from the gas phase and enriched in the hydrate phase when a gas mixture with a lower ethane concentration forms a hydrate[34,35]. The rapid formation and growth of hydrate crystals may reduce the local concentration of ethane. In a constant volume system, this reduction in local concentration would shift the thermodynamic equilibrium for hydrate formation, resulting in decreased subcooling compared to the bulk system and a reduced hydrate growth rate. In addition, the branches of dendritic crystals increase the exposed areas to higher concentrations of ethane, resulting in continued crystal growth. Dendritic growth is widely observed in crystal growth[36,37], and numerous explanations have been proposed to explain its occurrence[36]. As such, the dendritic morphology of the hydrate crystals observed herein further adds to the intriguing field of dendritic growth theory.

Another characteristic of hydrate films formed by gas mixtures with high methane mole fractions (0.834 and 0.923) is the heterogeneous shapes observed. We find both small gravel-like crystals and larger dendritic or leaf-like crystals in the main body of the film. It is quite interesting to note the near perfect polyhedral single crystals among the dendritic crystals formed by gas mixtures with the highest methane mole fraction of 0.923 (Figure 2). The edges of these polyhedral crystals are very clear and similar to single crystals of pure methane hydrate (white circled zone in Figure 2), suggesting they do not originate from the main dendritic crystals. (Instead, the polyhedral crystals in panels (e)–(h) in Figure 2 may originate from tiny crystals broken from the film crust). Hence, this phenomenon indicates the coexistence of sI and sII hydrates. The formation of sI hydrate is dominated by methane, while the formation of sII hydrate is dominated by both ethane and methane. The concomitant formation of sI and sII hydrates at the initial stage (the formation time is the same as the kinetic growth of hydrates at the gas bubble surface in Figure 2) has been observed by neutron diffraction and Raman spectroscopy for methane-ethane gas mixtures with methane mole fractions of 0.95 and 0.93[28,31], which is comparable to the gas composition in this study (methane mole fraction of 0.92). Our previous work on the Raman spectra of methane-ethane-tetrahydrofuran hydrates directly confirmed the coexistence of sI and sII[38]. The coexistence of sI and sII can also be inferred from the macroscopic partitioning of methane and ethane between the hydrate and vapour phases for systems with tetrahydrofuran in the liquid phase[34,39]. The appearance of methane hydrate crystals may be caused by the very high local concentration of methane near the main dendritic crystals due to the relatively faster consumption of ethane, as stated above.

The lateral growth rate (v_f) and initial thickness (δ) of the hydrate film measured at 278.0 K are shown in Tables S1 and S2 (see the Supporting Material) and are plotted in Figures 3 and 4. The lateral growth rate and initial thickness are calculated from the correlations proposed by Peng et al.[19] The lateral growth rate is correlated with $v_f = \psi \Delta T^{\frac{5}{2}}$, where ψ is a lateral growth rate parameter and ΔT is the degree of subcooling. For the initial hydrate film thickness, the correlation is $\delta = k/\Delta T$, where k is the inversely proportional coefficient. As shown in Figures 3 and 4, there is very good agreement between the experimental data and correlations.

Discussion

The various hydrate film morphologies observed in this study indicate that the kinetic behaviour of the hydrate film depends on the gas

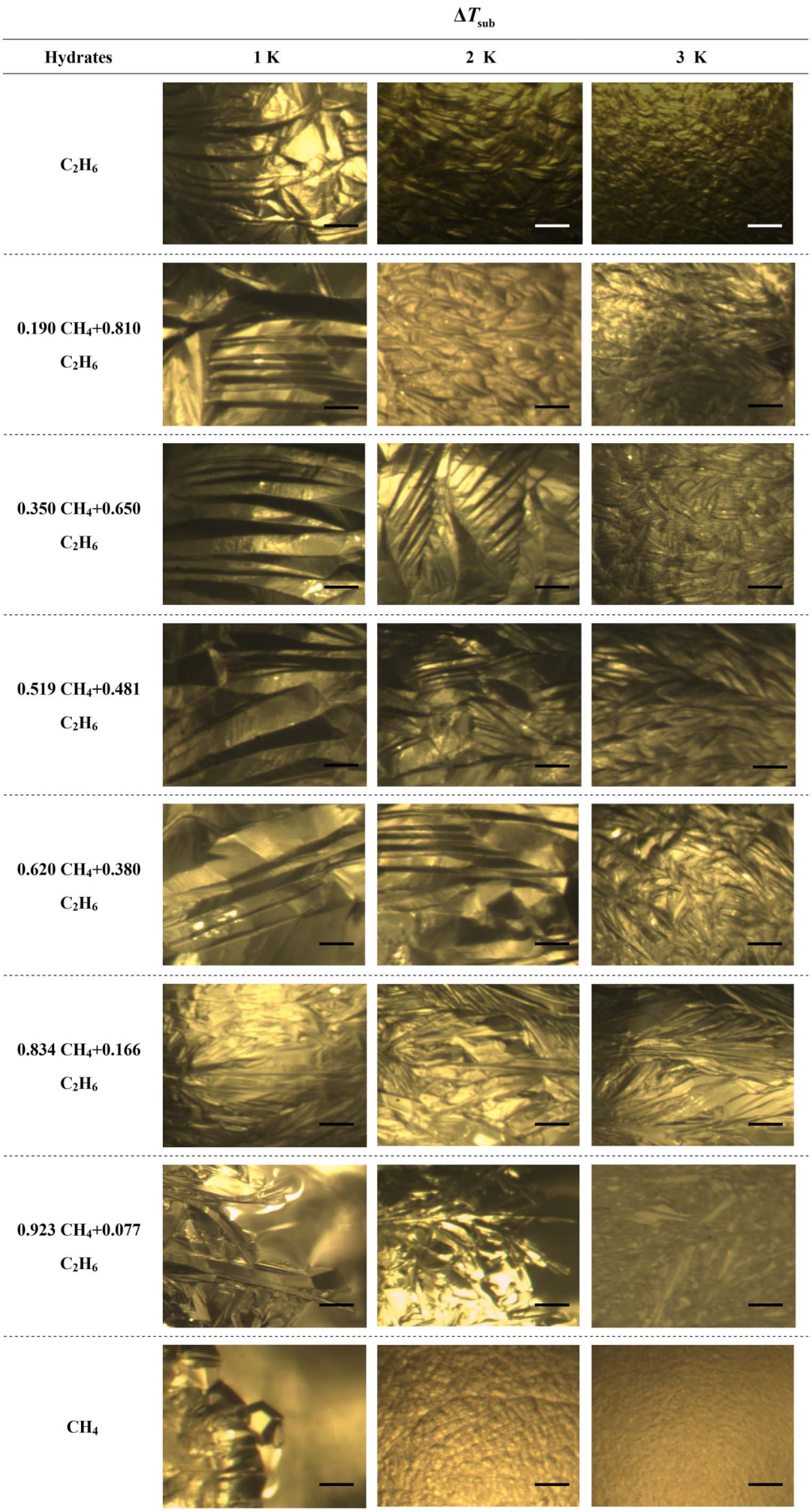

Figure 1 | Classification of hydrate film morphology based on ΔT_{sub} and composition of methane-ethane hydrate forming gases. The scale bars in the images correspond to 100 μm.

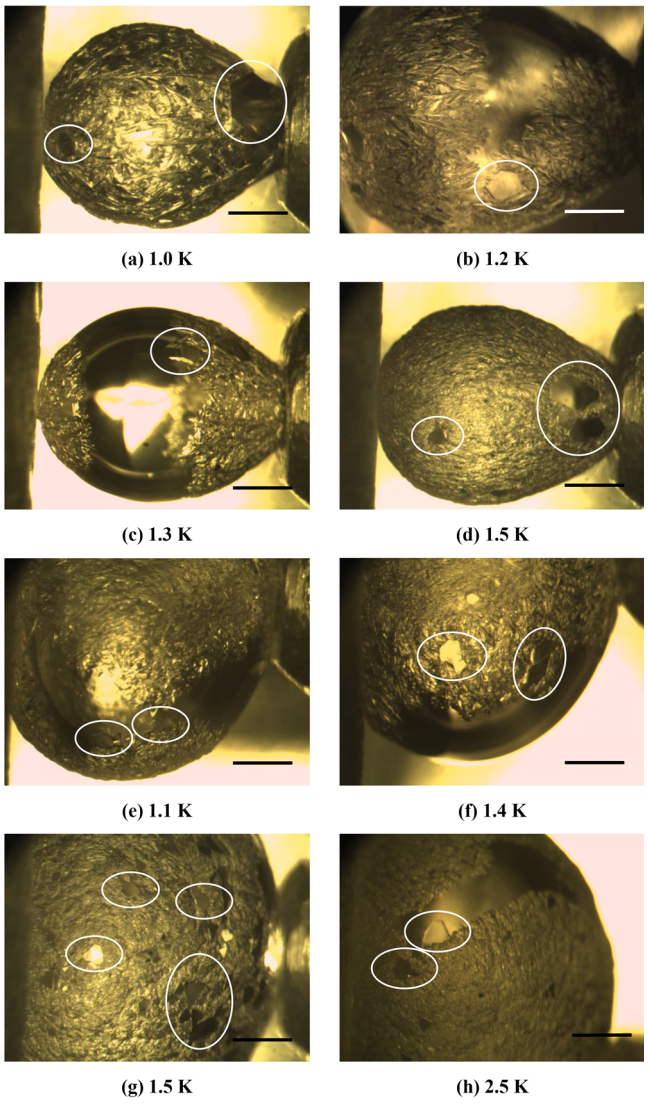

Figure 2 | The single crystals in the growth of hydrate films formed with methane-ethane hydrate forming gases with methane mole fraction of 0.923. Images (a)–(d) were recorded in the film lateral growth process and images (e)–(h) in the film regrowth process in the crust gap that was originated by supplying more gas to break the film crust after the gas bubble was fully covered by the hydrate film. The scale bars correspond to 1 mm.

composition and degree of subcooling. For example, there is little difference between the lateral growth rate data for methane hydrates in this work and the results obtained in our previous work using the same experimental method[19]. These growth rates are only slightly higher than those obtained at a planar water/methane interface[18,40]. However, these values are much lower than the lateral growth rates of methane hydrate films growing at the interface between methane and a sessile water droplet[41]. The differences in lateral growth rate for different systems (gas bubble or water droplet) should be caused by different volumetric growth rates, heat production rates, and heat transfer environments. For hydrate film growth at a given degree of subcooling (ΔT) in this work, the lateral growth rate and initial hydrate film thickness can be readily estimated using ψ and k, respectively, for a known composition of the hydrate forming gas. The values ψ and k for each hydrate-forming gas mixture are regressed from the experimental data in Figures 3 and 4 and plotted in Figure 5 (actual values are given in Tables S3 and S4 in the Supporting Material). As shown in Figure 5, the dependence of ψ

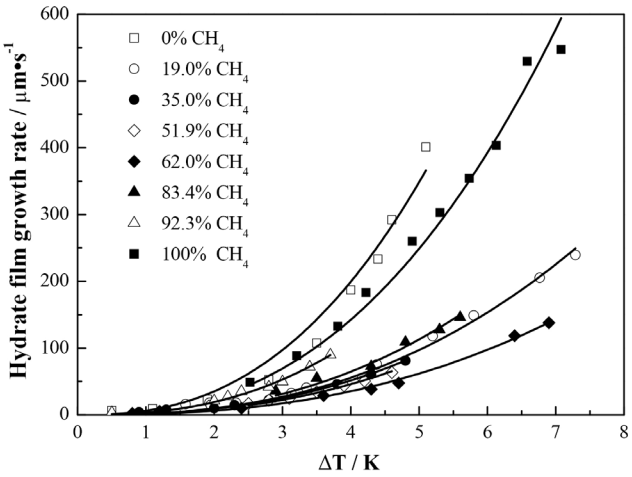

Figure 3 | Variation of lateral growth rate of hydrate film with subcooling for different hydrate forming gases. Solid lines denote the results calculated from the correlation $v_f = \psi \Delta T^{\frac{5}{2}}$.

and k on the gas composition is contrasting: the lateral growth rate of simple methane or ethane hydrate is higher than that of methane-ethane double hydrates, and the initial film thickness of simple methane or ethane hydrate is smaller than that of methane-ethane double hydrates for similar degree of subcooling. The maximum δ or minimum v_f occurs at a methane concentration of approximately 0.62. These results lead to the conclusion that a lower lateral growth rate leads to a thicker hydrate film, as more time is available for vertical development of the film front. Another way to interpret this result is that a thicker hydrate film is unfavourable for heat transfer and therefore lowers the lateral growth rate.

The product of δ and v_f provides the volumetric growth rate (r) of the hydrate at the gas-water-hydrate contact line,

$$r = \psi k \Delta T^{\frac{3}{2}} = \psi' \Delta T^{\frac{3}{2}} \quad (1)$$

where ψ' is the variation of the formation rate constant. The dependence of ψ' on the composition of the hydrate forming gas is shown in Figure 6 along with the volumetric hydrate growth rate. From the data, one can conclude that the volumetric growth rate of double hydrates is also lower than that of simple methane or ethane hydrate

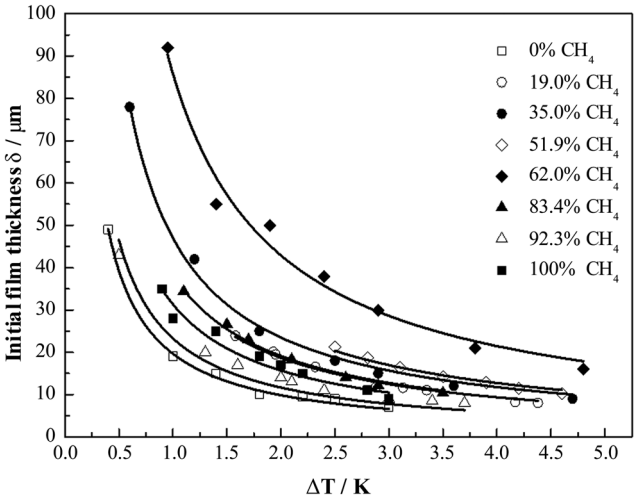

Figure 4 | Initial hydrate film thickness measured for different degrees of subcooling and hydrate forming gases. Solid lines denote the results calculated from the correlation $\delta = k/\Delta T$.

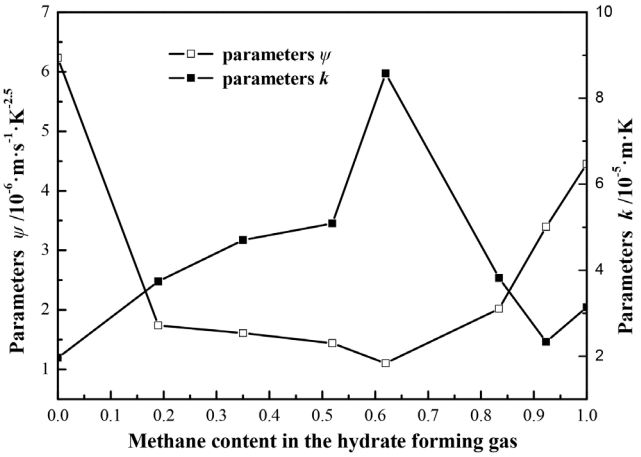

Figure 5 | Values determined for the parameters ψ and k for the different compositions of the hydrate forming gas.

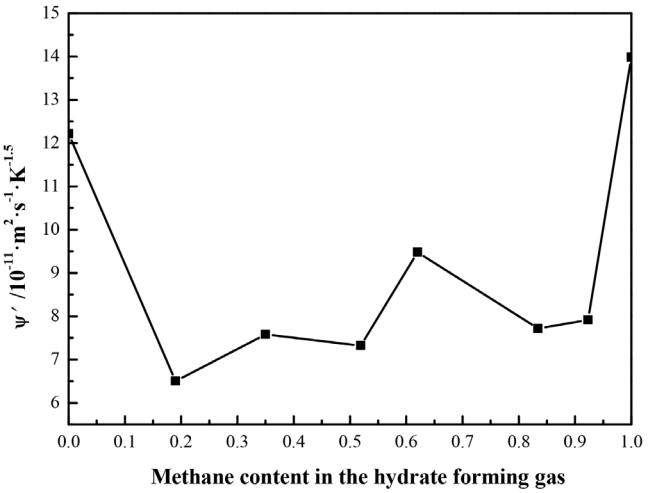

Figure 6 | Variation of formation rate constant (ψ') with composition of the hydrate forming gas.

at a given degree of subcooling. However, the influence of gas composition on the volumetric growth rate is not as pronounced as the influence of gas composition on the lateral growth rate. As discussed previously, the gas composition also affects the morphology and consequently the porosity of the hydrate film. Therefore, r is actually the apparent growth rate of the porous hydrate film and not the true volumetric growth rate of the hydrate lattice.

From the analysis of the growth rate and thickness of the hydrate film, it can be observed that the lateral hydrate film growth rate is determined by both the seeding rate of crystal seeds and the growth rate of the single crystal, which were determined from these morphology and kinetic studies. Generally, the seeding rate of crystal seeds is very low at low degrees of subcoolings so the lateral growth rate is controlled by the growth rate of a single crystal. In this case, the low lateral growth rate leads to a thicker hydrate film. Conversely, the seeding rate of crystal seeds is high at high degrees of subcooling and the lateral growth rate is controlled by both the seeding rate of crystal seeds and the growth rate of single crystal. This results in a higher lateral growth rate and a thinner hydrate film. In addition to the degree of subcooling, the gas composition also has a strong effect on the seeding rate of the crystal seeds. At a given degree of subcooling, three observations can be made: i) methane hydrates show the highest seeding rate; ii) the seeding rate decreases with increasing methane mole fraction ($y_{CH4} < 0.62$), suggesting that hydrate nucleation is controlled by ethane in these cases; and iii) the seeding rate increases with increasing methane mole fraction ($y_{CH4} > 0.62$), suggesting that hydrate nucleation is controlled by methane in these cases.

As stated previously, the gas composition dependence of the film morphology also indicates that the nucleation of hydrate crystal is dominated by ethane in the range $y_{CH4} < 0.62$, while it is dominated by methane or methane and ethane together in the range $y_{CH4} > 0.62$. In the range $y_{CH4} < 0.62$, the driving force for the formation of sI pure ethane hydrate crystal decreases with decreasing ethane concentration. Additionally, hydrate formation results in a local concentration of ethane near the film front lower than that of the bulk gas phase. This effect becomes more obvious with decreasing ethane concentration, as stated previously. These two factors may lead to a decreased seeding rate of the crystal seeds with decreasing ethane concentration in this concentration range. However, in the range $y_{CH4} > 0.62$, sII hydrate was assumed to be formed. In this case, as there are more small cavities in sII than in sI, methane likely has a greater contribution to hydrate nucleation, and therefore, the seeding rate increases with increasing methane concentration. These factors may explain why the lowest lateral growth rate occurs around $y_{CH4} =$ 0.62. The lowest lateral growth rate certainly corresponds to the largest thickness of the hydrate film.

In summary, the hydrate film growth processes of pure methane hydrate, pure ethane hydrate, and six methane-ethane double hydrates at the gas bubble/water interface were studied using microscopic visual methods. The morphologies, lateral growth rates, and thicknesses of the hydrate films were measured as a function of the gas composition and degree of subcooling. Based on these measurements, insight into the morphology and growth kinetic behaviour of methane-ethane hydrate films can be summarised as follows:

- (i) For $y_{CH4} = 0.0$ to 0.62, the morphologies of the hydrate films formed from gas mixtures are similar to that of simple ethane and quite different from that of pure methane. This result suggests that the nucleation and growth of the hydrate crystals is dominated by ethane. The observed crystals change from stratified to wheat ear-like with increasing subcooling.
- (ii) For $y_{CH4} = 0.834$ to 0.923, the crystal morphology becomes leaf-like or dendritic at lower degrees of subcooling, indicating the formation of sII hydrate. Additionally, polyhedral crystals like in pure methane hydrate can be observed among the main dendritic hydrate crystals, indicating the coexistence of sI and sII hydrates.
- (iii) The hydrate crystals formed at low degrees of subcooling always tend towards shapes that minimise heat or mass transfer and further favour hydrate film growth.
- (iv) The lateral hydrate film growth rate is controlled by the seeding rate of crystal seeds and the growth rate of single crystals. Both the degree of subcooling and gas composition strongly affect the seeding rate and therefore strongly affect the lateral hydrate film growth rate. At lower degrees of subcooling, the seeding rate of crystal seeds is very low and film growth is controlled by the growth of single crystals. At higher degrees of subcooling, the seeding rate of crystal seeds is high, and the lateral growth rate is controlled by both the seeding rate of crystal seeds and the growth rate of a single crystal. At a specified degree of subcooling, methane hydrates show the highest seeding rate. The seeding rate decreases with the decreasing ethane mole fraction in the range of y_{CH4} from 0.0 to 0.62, which further indicates the nucleation of hydrate is controlled by ethane in these cases. For higher y_{CH4} (>0.62), the seeding rate increases with decreasing ethane mole fraction, suggesting that hydrate nucleation is controlled by methane in these cases.
- (v) Lateral film growth rate and initial film thickness can be correlated by a kinetic model based on the assumption that heat transfer is the controlling step. The initial hydrate film thickness

and lateral hydrate film growth rate are found to vary inversely with the gas composition.

Methods

The experimental apparatus and procedure are the same as those used in our previous study[19,26]; details are provided in the Supporting Material. Double-distillated water was used in all measurements. Methane and ethane, both with a purity of 99.9% (mole basis), were provided by Beijing Beifen Gas Industry Corp. Six methane + ethane gas mixtures, with methane mole fractions of 0.190, 0.350, 0.519, 0.620, 0.834, and 0.923, were synthesized in our laboratory (mixed based on partial pressures) and their compositions were analysed by gas chromatography (HP6890). For all experiments performed, the temperature of the system was set to 278.0 K. The pressure for each experiment was varied to achieve the desired degree of subcooling.

1. Boswell, R. Is gas hydrate energy within reach? *Science* **325**, 956–957 (2009).
2. Nagai, Y. *et al.* Binary hydrogen-tetrahydrofuran clathrate hydrate formation kinetics and models. *AIChE J.* **54**, 3007–3016 (2008).
3. Sugahara, T. *et al.* Increasing hydrogen storage capacity using tetrahydrofuran. *J. Am. Chem. Soc.* **131**, 14616–14617 (2009).
4. Hu, Y. H. & Ruckenstein, E. Clathrate hydrogen hydrate–A promising material for hydrogen storage. *Angew. Chem. Int. Ed.* **45**, 2011–2013 (2006).
5. Florusse, L. J. *et al.* Stable low-pressure hydrogen clusters stored in a binary clathrate hydrate. *Science* **306**, 469–471 (2004).
6. Schuth, F. Technology: Hydrogen and hydrates. *Nature* **434**, 712–713 (2005).
7. Kumar, R., Linga, P., Moudrakovski, I., Ripmeester, J. A. & Englezos, P. Structure and kinetics of gas hydrates from methane/ethane/propane mixtures relevant to the design of natural gas hydrate storage and transport facilities. *AIChE J.* **54**, 2132–2144 (2008).
8. Sloan, E. D. Fundamental principles and applications of natural gas hydrates. *Nature* **426**, 7 (2003).
9. Lehmkuhler, F. *et al.* The carbon dioxide−water interface at conditions of gas hydrate formation. *J. Am. Chem. Soc.* **131**, 585–589 (2008).
10. Liang, S. & Kusalik, P. G. The mobility of water molecules through gas hydrates. *J. Am. Chem. Soc.* **133**, 1870–1876 (2011).
11. Watanabe, S., Saito, K. & Ohmura, R. Crystal growth of clathrate hydrate in liquid water saturated with a simulated natural gas. *Cryst. Growth Des.* **11**, 3235–3242 (2011).
12. Saito, K., Kishimoto, M., Tanaka, R. & Ohmura, R. Crystal growth of clathrate hydrate at the interface between hydrocarbon gas mixture and liquid water. *Cryst. Growth Des.* **11**, 295–301 (2011).
13. Lee, J. D., Susilo, R. & Englezos, P. Methane-ethane and methane-propane hydrate formation and decomposition on water droplets. *Chem. Eng. Sci.* **60**, 4203–4212 (2005).
14. Sun, C. Y. *et al.* The growth kinetics of hydrate film on the surface of gas bubble suspended in water or aqueous surfactant solution. *J. Cryst. Growth* **306**, 491–499 (2007).
15. Mori, Y. H. Estimating the thickness of hydrate films from their lateral growth rates: application of a simplified heat transfer model. *J. Cryst. Growth* **223**, 206–212 (2001).
16. Mochizuki, T. & Mori, Y. H. Clathrate-hydrate film growth along water/hydrate-former phase boundaries--numerical heat-transfer study. *J. Cryst. Growth* **290**, 642–652 (2006).
17. Uchida, T., Ebinuma, T., Kawabata, J. i. & Narita, H. Microscopic observations of formation processes of clathrate-hydrate films at an interface between water and carbon dioxide. *J. Cryst. Growth* **204**, 348–356 (1999).
18. Freer, E. M., Sami Selim, M. & Sloan, E. D. Methane hydrate film growth kinetics. *Fluid Phase Equilib.* **185**, 65–75 (2001).
19. Peng, B. Z. *et al.* Hydrate film growth on the surface of a gas bubble suspended in water. *J. Phys. Chem. B* **111**, 12485–12493 (2007).
20. Servio, P. & Englezos, P. Morphology of methane and carbon dioxide hydrates formed from water droplets. *AIChE J.* **49**, 269–276 (2003).
21. Kobayashi, I., Ito, Y. & Mori, Y. H. Microscopic observations of clathrate-hydrate films formed at liquid/liquid interfaces. I. Morphology of hydrate films. *Chem. Eng. Sci.* **56**, 4331–4338 (2001).
22. Ohmura, R., Matsuda, S., Uchida, T., Ebinuma, T. & Narita, H. Clathrate hydrate crystal growth in liquid water saturated with a guest substance: Observations in a methane + water system. *Cryst. Growth Des.* **5**, 953–957 (2005).
23. Sugaya, M. & Mori, Y. H. Behavior of clathrate hydrate formation at the boundary of liquid water and a fluorocarbon in liquid or vapor state. *Chem. Eng. Sci.* **51**, 3505–3517 (1996).
24. Ohmura, R., Kashiwazaki, S. & Mori, Y. H. Measurements of clathrate-hydrate film thickness using laser interferometry. *J. Cryst. Growth* **218**, 372–380 (2000).
25. Hirai, S., Tabe, Y., Kuwano, K., Ogawa, K. & Okazaki, K. E. N. MRI measurement of hydrate growth and an application to advanced CO_2 sequestration technology. *Ann. N.Y. Acad. Sci.* **912**, 246–253 (2000).
26. Li, S. L. *et al.* Initial thickness measurements and insights into crystal growth of methane hydrate film. *AIChE J.* **59**, 2145–2154 (2013).
27. Chen, G. J. & Guo, T. M. Thermodynamic modeling of hydrate formation based on new concepts. *Fluid Phase Equilib.* **122**, 43–65 (1996).
28. Murshed, M. M. & Kuhs, W. F. Kinetic studies of methane-ethane mixed gas hydrates by neutron diffraction and Raman spectroscopy. *J. Phys. Chem. B* **113**, 5172–5180 (2009).
29. Subramanian, S., Kini, R. A., Dec, S. F. & Sloan Jr, E. D. Evidence of structure II hydrate formation from methane + ethane mixtures. *Chem. Eng. Sci.* **55**, 1981–1999 (2000).
30. Subramanian, S., Ballard, A. L., Kini, R. A., Dec, S. F. & Sloan, E. D. Structural transitions in methane + ethane gas hydrates – Part I: upper transition point and applications. *Chem. Eng. Sci.* **55**, 5763–5771 (2000).
31. Ohno, H., Strobel, T. A., Dec, S. F., Sloan, E. D., Jr. & Koh, C. A. Raman studies of methane-ethane hydrate metastability. *J. Phys. Chem. A* **113**, 1711–1716 (2009).
32. Murshed, M. M., Schmidt, B. C. & Kuhs, W. F. Kinetics of methane-ethane gas replacement in clathrate-hydrates studied by time-resolved neutron diffraction and Raman spectroscopy. *J. Phys. Chem. A* **114**, 247–255 (2010).
33. Ballard, A. L. Structural transitions in methane ethane gas hydrates – Part II: modeling beyond incipient conditions. *Chem. Eng. Sci.* **55**, 5773–5782 (2000).
34. Zhang, L. W. *et al.* The partition coefficients of ethylene between hydrate and vapor for methane + ethylene + water and methane + ethylene + SDS + water systems. *Chem. Eng. Sci.* **60**, 5356–5362 (2005).
35. Liu, H. *et al.* Experimental studies of the separation of C2 compounds from CH_4 + C_2H_4 + C_2H_6 + N_2 gas mixtures by an absorption−hydration hybrid method. *Ind. Eng. Chem. Res.* **52**, 2707–2713 (2013).
36. Glicksman, M. Mechanism of dendritic branching. *Metall. Mater. Trans. B* **43**, 207–220 (2012).
37. Glicksman, M. [Chapter 13, Dendritic growth] *Principles of solidification: An introduction to modern casting and crystal growth concepts* [305–343] (Springer Verlag, New York, 2010).
38. Sun, C. Y., Chen, G. J. & Zhang, L. W. Hydrate phase equilibrium and structure for (methane + ethane + tetrahydrofuran + water) system. *J. Chem. Thermodyn.* **42**, 1173–1179 (2010).
39. Ma, Q. L., Chen, G. J., Ma, C. F. & Zhang, L. W. Study of vapor-hydrate two-phase equilibria. *Fluid Phase Equilib.* **265**, 84–93 (2008).
40. Kitamura, M. & Mori, Y. H. Clathrate-hydrate film growth along water/methane phase boundaries–an observational study. *Cryst. Res. Technol.* **48**, 511–519 (2013).
41. Tanaka, R., Sakemoto, R. & Ohmura, R. Crystal growth of clathrate hydrates formed at the interface of liquid water and gaseous methane, ethane, or propane: variations in crystal morphology. *Cryst. Growth Des.* **9**, 2529–2536 (2009).

Acknowledgments

This project was financially support by the National 973 Project of China (No. 2012CB215005) and the National Natural Science Foundation of China (Nos. 20925623, U1162205, 51376195).

Author contributions

C.Y.S. and G.J.C. proposed and supervised the entire project. S.L.L., Z.Y.L. and B.L. performed the experiments and analysis. S.L.L., C.Y.S., G.J.C. and A.K.S. contributed to the discussion and interpretation of the results, and writing of this manuscript.

Additional information

Supplementary information accompanies this paper at http://www.nature.com/scientificreports

Competing financial interests: The authors declare no competing financial interests.

How to cite this article: Li, S.-L. *et al.* New Observations and Insights into the Morphology and Growth Kinetics of Hydrate Films. *Sci. Rep.* **4**, 4129; DOI:10.1038/srep04129 (2014).